Salvador, FJ.; De La Morena, J.; Crialesi Esposito, M.; Martínez López, J. (2018). Comparative study of the internal flow in diesel injection nozzles at cavitating conditions at different needle lifts with steady and transient simulations approaches. Proceedings of the Institution of Mechanical Engineers Part D Journal of Automobile Engineering. 232(8):1060-1078. https://doi.org/10.1177/0954407017725672

Proc IMechE Part D: J Automobile Engineering 2018, Vol. 232(8) 1060–1078

COMPARATIVE STUDY OF THE INTERNAL FLOW IN DIESEL INJECTION NOZZLES AT CAVITATING CONDITIONS AT DIFFERENT NEEDLE LIFTS WITH STEADY AND TRANSIENT SIMULATIONS APPROACHES.

Salvador, FJ[1] (*), De la Morena, J. [1], Crialesi-Esposito, M. [1], Martínez-López, J.[2]

[1]CMT-Motores Térmicos, Universitat Politècnica de València

Camino de Vera s/n, E-46022, Valencia, Spain.

[2] Williams Grand Prix Engineering Limited

Grove, Wantage, Oxfordshire, OX12 0DQ

(*) Corresponding author:

Dr. F. Javier Salvador, fsalvado@mot.upv.es

CMT-Motores Térmicos, Universitat Politècnica de València

Camino de Vera s/n, E-46022 Spain.

Telephone: +34-963879659

FAX: +34-963877659

ABSTRACT

The motion of the needle during the injection process of a Diesel injector has a marked influence on the internal flow, the fuel characteristics at the nozzle exit, the spray pattern and the fuel-air mixing process. The current paper is focused on the computational study of the internal flow and cavitation phenomena during the injection process, including the opening where the needle is

working at partial lifts. This study has been performed with a homogeneous equilibrium model (OpenFOAM) customized by the authors to simulate the real motion of the needle.

The first part of the study covers the analysis of the whole injection process with moving mesh using the boundary conditions provided by a 1D model of the injector created in AMESim. This one-dimensional model has offered the possibility of reproducing the movement of the needle with the real lift law and the real injection pressure evolution during the injection. Thus, it has been possible to compare the injection rate profiles provided by OpenFOAM against those obtained in AMESim and experimentally. The second part compares the differences in mass flow, momentum flux, effective velocity and cavitation appearance between steady (fixed lifts) and transient (moving mesh) simulations. The aim of this comparison is to establish the differences between these two approaches. On the one hand, a more realistic one, by means of transient simulations of the injection process, where the needle movement is taken into account. On the other hand, the use of steady simulations at partial needle lifts. This analysis could be of the interest of researchers devoted to the study of diesel injection process since it could help to delimit the uncertainties involved to using the second approach (easier to be carried out) versus the first one, which it is supposed to provide more realistic results.

KEYWORDS

Cavitation, needle lift, moving mesh, diesel, nozzle, CFD.

NOMENCLATURE

a: speed of sound

C_{μ}: constant for turbulent viscosity calculation

$C_{\varepsilon 1}$: constant for ε transport equation calculation

$C_{\varepsilon 2}$: constant for ε transport equation calculation

k: turbulent kinetic energy

$\dot{m}$: mass flow

$\dot{M}$: momentum flux

p: pressure

P_{back}: backpressure

P_{inj}: injection pressure

P_k: production of turbulent kinetic energy

t: time

u: velocity

Greek symbols:

γ: vapour fraction

ε: turbulence dissipation rate

μ: fluid viscosity

μ_T: turbulent viscosity

σ_ε: constant for ε transport equation calculation

σ_k: constant for k transport equation calculation

ρ: fluid density

$\rho_{l\,sat}$: liquid density at saturation

$\rho_{v\,sat}$: vapour density at saturation

Ψ: fluid compressibility

Subscripts:

l: liquid

v: vapour

1. INTRODUCTION

Over the last decades, the injection pressure used in automotive diesel engines has gradually risen in order to improve the atomization of the spray. The use of injection pressures that can easily arrive up to 200 MPa promotes under certain conditions the cavitation phenomenon within the injector nozzles. It is well know that cavitation can cause significant damages in turbines or propellers. However, in diesel engines cavitation contributes to increase the spray angle, boosting the air-fuel mixing process [1]–[7]. Furthermore, the existence of vapour bubbles inside the injection nozzles increases the maximum speed of the fuel due to the reduction in the friction with the walls [8], [9], and the smaller effective cross section available for the fuel in liquid phase [8], [10].

Unfortunately, the experimental study of the cavitation in diesel injection nozzles presents big difficulties derived mainly from their typical dimensions (with diameters below 200 μm and lengths around 1 mm) and the high velocities of the fuel flowing inside. Furthermore, the huge influence of the geometric characteristics of the nozzle [11]–[17] complicates even more the study of the injection process, since the motion of the needle during the injection changes completely the internal geometry of the nozzle. This subject is precisely becoming more and more significant over the last years due to the use of pre- and post-injections to reduce the noise and the emissions of the combustion engines [18]–[20].

With the increase of the injections per cycle seen over the last years, the needle of the injector often works at partial needle lifts, without reaching its maximum lift. This fact has awaken the interest from many researchers to understand in detail the characteristics of the flow at partial

needle lifts, stimulating the publication of computational studies that have evidenced the influence of the needle position on the internal flow and cavitation phenomenon.

Blessing et al. [21] published the results of their investigation about the internal flow and cavitation phenomenon, and its influence on the spray development and mixing process. This investigation was performed on full scale transparent nozzles in pressure conditions similar to those existing in diesel combustion engines. Pictures of the vapour bubbles during the opening and closing process of the injector were obtained for several injection systems and nozzles with different conicity. Those pictures were compared with CFD results obtained with AVL-FIRE, fact that allowed the detailed study of the cavitation development according to the needle displacement. The same code, classified as a two fluid model, was used by Masuda et al. [22] to study the cavitation development in a multihole VCO nozzle. Masuda et al. analysed the transient behaviour of the cavitation during the opening and closing process, and investigated about the formation of tiny vortexes and eddies within the discharge orifices. The results obtained at the nozzle outlet (velocity, vapour phase, turbulence, etc.) were used as an inlet boundary condition for the simulation of the primary atomization of the spray and the mixing process with the air.

A similar study of the spray was carried out by Soriano et al. [23] with ANSYS-CFX . In this case, the code was validated with experimental mass flow measurements at different needle lifts during the injector opening. The experimental data included also measurements at maximum needle lift for different injection pressures, which were used to deal with the analysis of the critical cavitation conditions. From the internal flow results, Soriano et al. completed the study with the simulation of the spray, paying special attention to its penetration and angle, and the size of the droplets that form the spray. Som et al. [24] also investigated the influence of the injection pressure, fuel properties and needle position on the cavitation development in a minisac nozzle. In this work, the authors simulated, with the commercial code Fluent [25], the internal flow at partial needle lifts without modelling the mesh motion. Som et al. showed significant differences in the cavitation appearance developed inside the nozzle orifice due to the fuel properties as well as the needle position. More recently, Salvador et al. [26], [27] published the results of their

investigations about the influence of the needle lift position on the internal flow and cavitation phenomenon. Both the works included an extensive validation with experimental data and focused on the evolution of the internal flow, the turbulence development (vorticity, turbulence-cavitation interaction and turbulent structures) and the flow characteristics at the nozzle outlet with the needle position.

Other authors like Oda et al. [28] published also an investigation about the effect of the needle position on the internal flow and spray angle. However, the aim of this study was not the needle lift, but its eccentricity. Oda et al. observed experimentally in Diesel VCO nozzles a reduction of the spray angle with the entrance of air coming from the combustion chamber. This phenomenon was also detected computationally by means of the simulation of the flow with a VOF model implemented in STAR-CD. The effects of the needle eccentricity were also studied computationally with OpenFOAM by Salvador et al. [29], who observed important hole to hole differences in the internal flow and strong variations of the cavitation generated among the orifices. Salvador et al. showed that an eccentric position of the needle produces lower values of mass flow, momentum flux and effective velocity at the nozzle exit. Similarly, Battistoni et al. [30] evaluated the impact of off-axis needle motion using CONVERGE software, showing that the hole-to-hole variations induced by this phenomenon were particularly important at low and mid needle lift conditions.

Chiavola et al. [31] also studied the effect of the needle eccentricity on the internal flow with the CFD tool AVL-FIRE, using needle lift laws coming from a 1D model created in AMESim [32]. Both studies demonstrated that a radial displacement of the needle could lead to notable differences among the orifices of the injector in terms of velocity of the fluid or location and extension of the vapour region. Those differences were minimum at fully needle lift conditions and rose sharply as the needle moves down. Another CFD work carried out using AMESim to get the real needle lift law was published by Lee et al. [33], who compared the differences in the internal flow development between a piezoelectric and a solenoid injector. The faster response of the piezoelectric injector needle during the opening process caused more cavitation and therefore,

a velocity rise of the fuel. Lee et al. showed also experimentally how this velocity rise and the faster needle opening had effects on the spray development, growing considerably faster compared with the solenoid injector spray. Considering the great usefulness of AMESim as a tool to know with accuracy parameters like the evolution of the pressure injection or the needle lift over the injection, R. Marcer et al. [34] coupled that 1D tool to a 3D software like EOLE. This new tool, validated in real nozzles with experimental data coming from Renault, showed good results in the prediction of the mass flow injected.

The present paper attempts to go beyond, using AMESim to get the transient pressure injection and the needle lift to study the evolution of the mass flow as well as the momentum flux, effective velocity and cavitation over the injection event. For this purpose, with a customized version of a standard OpenFOAM solver is used. Firstly, the paper introduces the main equations of the cavitation and turbulence models together with the major changes performed in the standard OpenFOAM solver to simulate the needle motion. Secondly, all the settings necessary to run the simulations (nozzle geometry, mesh parameters, boundary conditions, fuel properties, etc.) are described before going into detail in the results of the investigation. Those results have been split in two sections: section 4 shows how the 1D model of the injector created in AMESim is able to supply realistic boundary conditions for simulating the whole injection process. This section includes also a comparison of the injection rate obtained experimentally against those obtained with AMESim and OpenFOAM. In section 5, a comparative analysis on the internal flow with fixed needle lifts (steady simulations) and mesh motion (transient simulations) is performed. The aim of this comparison is to clearly establish what are the differences in the analysis of the inner nozzle flow in diesel nozzles when two different approaches are used. On the one hand, a more realistic one, by means of transient simulations of the initial part of the injection process with a realistic needle movement. On the other hand, the use of steady simulations at different partial needle lifts, which is a simplification of the real injection process. Finally, the main conclusions of the study are drawn in the last section of the paper.

2. DESCRIPTION OF THE CFD APPROACH

2.1 Cavitation Modelling

Considering the characteristics of the internal flow within the injection nozzles, with high pressure gradients and high velocities, the use of a homogeneous equilibrium model seems to be the most suitable approach to model the cavitation phenomena [35]. For that reason, the authors have chosen a model based on Schmidt model [36] implemented in OpenFOAM (rasCavitatingFoam) and already validated by the authors with experimental data in calibrated orifices, both for single and multihole nozzles [37]–[40].

The model assumes that the liquid and vapour phases are perfectly mixed in each cell of the mesh and the temperature of the fluid remains constant. In HEM models, the assumptions of local kinematic equilibrium (local velocity is the same for both phases) and local thermodynamic equilibrium (temperature, pressure and free Gibbs enthalpy equality between phases) are made. This kind of model cannot reproduce strong thermodynamic or kinetic non-equilibrium effects, but it is often used for numerical simulations due to its simplicity and numerical stability. These two advantages are the main reasons why this model was chosen by the authors.

The main equations are the continuity equation (Eq. 1), the momentum equation (Eq. 2) and a barotropic equation of state (Eq. 3), which links the density of the fluid with its pressure through the compressibility:

$$\frac{\partial \rho}{\partial t} + \nabla \cdot (\rho \vec{u}) = 0 \tag{1}$$

$$\frac{\partial (\rho \vec{u})}{\partial t} + \nabla \cdot (\rho \frac{\vec{u}\vec{u}}{2}) = -\nabla p + \nabla \cdot (\mu \nabla \vec{u}) - \nabla \tau \tag{2}$$

$$\frac{D\rho}{Dt} = \Psi \frac{Dp}{Dt} \tag{3}$$

The compressibility of the fluid is defined as the inverse of the speed of sound to the squared power (Eq. 4) and is calculated with a linear expression (Eq. 5) as a function of the compressibility of the pure liquid, the compressibility of the pure vapour and the amount of vapour in each cell, represented with the variable γ:

$$\Psi = \frac{1}{a^2} \tag{4}$$

$$\Psi = \gamma \cdot \Psi_v + (1-\gamma) \cdot \Psi_l \tag{5}$$

$$\gamma = \frac{\rho - \rho_{lsat}}{\rho_{vsat} - \rho_{lsat}} \tag{6}$$

The use of a linear expression to calculate the compressibility of the fluid instead of using other models based on Wallis [41] or Chung [42] investigations, which are physically more realistic, is justified by convergence and numerical stability reasons. Similar argument has been applied for the calculation of the viscosity of the mixture as a function of the existing amount of liquid and vapour:

$$\mu = \gamma \cdot \mu_v + (1-\gamma) \cdot \mu_l \tag{7}$$

For the current study, as in other similar works in the literature [7], [24], [30], energy conservation equation is not included into the simulation, so the flow is considered to be isothermal. This assumption can be considered as reasonable for low and moderate injection pressures, where the temperature change along the nozzle is reduced. Nevertheless, at very high injection pressures, it has to be considered that the addition energy conservation equation can play a role on the nozzle flow dynamics. This will be the topic of future investigations by the authors.

2.2 Turbulence Modelling.

There are many experimental and computational works which show that the turbulence plays an important role on the flow development in injection nozzles [43]–[46]. The turbulence effects can be introduced in the CFD models mainly by three different approaches, depending on the desired accuracy and the computational resources available: DNS (Direct Numerical Simulation) [47], LES (Large Eddy Simulation) [48], [49] or RANS (Reynolds Averaged Navier-Stokes) [50].

For the current investigation, considering the complexity of the cavitating flow and the computational cost of simulating the needle motion, a RANS model has been used. One of the most common used RANS models is the "*k-ε* model", which is a two-equation model, as it solves

additional transport equations for two turbulent variables. However, since its development in 1972, the *k-ε* model has evolved in different versions (realizable, RNG, etc.) with the idea of being able to adapt better to the particularities of each application in fluid dynamics. In this sense, due to the high pressure and velocity gradients existing in diesel injection nozzles, the authors have chosen a RNG k-ε model developed by Yakhot et al.[51]. This model solves an additional transport equation for the turbulent kinetic energy (*k*) and another transport equation for the turbulence dissipation rate (*ε*):

$$\frac{\partial}{\partial t}(\rho k)+\frac{\partial}{\partial x_i}(\rho k u_i)=\frac{\partial}{\partial x_j}\left[\left(\mu+\frac{\mu_T}{\sigma_k}\right)\frac{\partial k}{\partial x_j}\right]+P_k-\rho\varepsilon-2\rho\varepsilon\frac{k}{a^2} \tag{8}$$

$$\frac{\partial}{\partial t}(\rho \varepsilon)+\frac{\partial}{\partial x_i}(\rho \varepsilon u_i)=\frac{\partial}{\partial x_j}\left[\left(\mu+\frac{\mu_T}{\sigma_\varepsilon}\right)\frac{\partial \varepsilon}{\partial x_j}\right]+C_{1\varepsilon}^{*}\frac{\varepsilon}{k}P_k-C_{2\varepsilon}\rho\frac{\varepsilon^2}{k} \tag{9}$$

being the turbulent viscosity:

$$\mu_t=\rho C_\mu\frac{k^2}{\varepsilon} \tag{10}$$

where C_μ = 0.0845, $C_{\varepsilon 1}$ = 1.42, $C_{\varepsilon 2}$ = 1.68 and $\sigma_k = \sigma_\varepsilon$ = 0.72.

2.3 Modification of the standard OpenFoam code to simulate the motion of the needle.

One of the most attractive features of OpenFOAM is the possibility of modifying any model already implemented to adapt it to the peculiarities of each problem. In this case, the code has been modified to allow the motion of the mesh during the run. It is important to highlight this achievement not only because it gives the user the opportunity of considering the dynamic effects of the needle motion on the calculations, but also because the new version of the code is able to simulate the whole injection process (including the opening and closing). Consequently, it is possible to obtain results for any needle lift in only one simulation. That fact implies significant savings in computational cost and preprocessing time (creating the geometry and generating the mesh) compared to multiple fixed-lift simulations. In this sense, if for the simulation of fixed needle lifts it was necessary to create and mesh a different geometry for each needle lift, while

with the new version of the code the user only needs to create and mesh the initial geometry. That geometry will be deformed during the run to reproduce the different needle positions.

The algorithm implemented in the cavitation model allows the motion of any region previously defined according to a certain velocity law. Its vertical or horizontal movement is based on the deformation of the cells of the mesh. As an example, Figure 1 and 2 show a detailed view of the domain simulated together with the evolution of the mesh for different needle lifts obtained after the vertical motion of the regions corresponding to the needle wall.

The method chosen for the mesh motion is based on the OpenFOAM sub-class called "dynamicMotionSolverFvMesh", corresponding to the library "libDynamicFvMesh.so". This mesh manipulation approach solves the mesh motion equations by stretching or squeezing the cells of the domain according to the submodel specified. For this particular application, the authors have used the velocityLaplacian submodel, where the equations of the cell motion are solved based on the laplacian of the diffusivity and the velocity of the cells.

From the perspective of the mesh, the most critical part of the simulation corresponds with the last instants before the needle closes the injector because the cells located between the needle and the nozzle wall are strongly deformed and squashed. Obviously, the full closing of the injector is impossible to achieve because the cells cannot be removed or have zero volume. For that reason, the motion of the needle is limited up to a minimum lift of 5 μm. With regard to the configuration of the needle motion, the movement is introduced in the model using a text file with two columns where the velocity of the needle is defined for each time. Thus, the user can introduce simple needle lift laws to simulate the opening and closing stages with a constant speed or complex needle lift laws to simulate multiple injections where the needle is opening and closing the injector repeatedly.

3. SIMULATION SETTINGS: NOZZLE, MESH, BOUNDARY CONDITIONS AND FUEL PROPERTIES

The study of the influence of the needle lift on the internal flow has been performed in a real microsac multihole nozzle. The main important geometric characteristics were obtained by silicon moulds following the methodology described by Macian et al. [52]. Its orifices (six in total) present approximately the same inlet and outlets diameters (170 μm), fact that can promote the cavitation phenomena as suggested on many investigations published over the last years [11][53][54]. Other important dimensions for the flow development are the curvature radius at the orifice inlet (13 μm) and the orifice length (1 mm). The simulated domain (see Figure 1) has been simplified to one of the six orifices assuming that the nozzle is completely symmetric. This simplification reduces drastically the computational cost without severely affecting the accuracy of the results and the validity of the conclusions derived from this investigation. Nevertheless, it has to be considered that in real conditions small deviations in the orifices dimensions and a non-fully symmetric needle motion may induce some hole-to-hole dispersion that could be investigated in the future with a complete nozzle geometry.

The resulting simplified geometry has been meshed with ANSYS - ICEM CFD with hexahedral elements according to previous sensitivity studies performed in similar diesel injector nozzles [12], paying special attention to the area near the orifice inlet since it is there where cavitation usually starts. The cell size used on the orifice walls is about 1.15 μm and rises gradually up to 9 μm in the orifice core. The sac and the upstream domain have been meshed with a variable cell size for the different geometries simulated for the steady simulations (10, 20, 30, 40, 50, 75 and 100 μm) based on keeping constant the ratio wall cell size/needle lift. Anyway, the maximum cell size allowed upstream the orifice was set to 10 μm, giving rise to meshes of around 84000 cells.

For the moving mesh simulations, the cell size chosen for the entire domain is similar although the process to generate the mesh is different. In this case, the mesh is generated for an intermediate needle lift to minimize the deformation of the cells when the needle is working at fully needle lift conditions or at low lifts. For each new nozzle, the mesh is moved to the highest and lowest needle

position before the start of the simulation to check the cells quality with the OpenFOAM utility "checkMesh" and guarantee its validity.

Due to the small cell sizes used close to the wall, no wall functions were used for the simulations. As an indicator of the mesh quality, the mean values for the dimensionless distance, y+ was evaluated in the whole domain. A distinction has been made between the orifice (where most severe gradients of pressure and velocity are expected) and the rest of the geometry because of the different refinement requirements. The mean y+ value in the orifice was 1, whereas the same value for the rest of the walls was 5.

The boundary conditions applied have been chosen to reproduce accurately the real behaviour of the flow and ensure a good convergence of the solution, whose residuals are always below 1e-5. The main boundary conditions can be summarized as follows:

- Injection pressure. The injection pressure defined in the simulations corresponds to the difference between the common rail pressure and the losses located in the downstream line and the injector holder. The pressure is set in the CFD model as a uniform value, which can be constant over time (as used for the steady-state simulations in section 4) or variable to reproduce the real evolution of the pressure over the whole injection process (introduced for the transient simulations in section 5) .
- Backpressure. The backpressure corresponds to the pressure registered in the discharge chamber or the combustion chamber, which can be experimentally measured and controlled. In contrast with the injection pressure, the backpressure is set as a mean value boundary condition. Thus, the vapour bubbles whose pressure is below the saturation pressure (5400 Pa) can reach the nozzle exit although the outlet pressure value chosen is higher. Indeed, all the simulations presented in this paper have been run with a backpressure 3 MPa, so no vapour could reach the orifice outlet if uniform boundary condition would have applied.

- Walls. The walls have been modelled with a non-slip boundary condition, so the velocity of the fuel relative to the walls will be zero.
- Symmetry planes. As only one sector of the nozzle has been modelled (60°), a symmetry condition has been set on both sides of the sector.
- Needle wall. As mentioned in section 2.3, a displacement boundary condition has been applied in those simulations where the motion of needle has been modelled to reproduce the opening and closing stages of the injector. The mesh nodes corresponding to the needle wall can be moved upwards or downwards according to the lift law (see Figure 1).

As far as the fluid properties are concerned, the density and viscosity values in liquid phase matches with the properties of the fuel "Repsol CEC RF-06-99" at 23 ºC (see Table 1). This fuel was used to get the experimental injection rates showed in section 4 in order to validate the computational results obtained with OpenFOAM and AMESim.

4. COUPLING CFD SIMULATIONS WITH AMESIM RESULTS.

To simulate the needle motion it is very important to know in depth the right boundary conditions since they affect the validity and accuracy of the results obtained by OpenFOAM. For that reason, the injector used in the current investigation (Bosch CRI2.2.) has been modelled in AMESim platform. This 1D model of the injector has given the opportunity of knowing the real needle lift law and the injection pressure for any working condition. Only in that way it is possible to simulate in CFD the real injection process.

4.1 AMEsim Model

The 1D model of the injector created in AMESim can be split in three main groups: electrovalve, injector holder and nozzle. A detailed description of the methodology followed to obtain the 1D model is given in [55]. This methodology is based on a functional, hydraulic and geometrical characterization of the different components that comprise the system. Just as an example of this methodology, the part of the model related to the nozzle is depicted in Figure 3 where it is also

shown a picture of the internal lines and volumes. This part of the whole model would be linked to the injector holder model by means of a hydraulic connection (NL1) and a mechanical connection that represents the mechanical contact between the needle and the rod.

The fuel coming from the injector holder flows along the line NL1 towards the volume NV1, which is connected to the piston NP1. The NP1 piston simulates the pressure force of the fuel acting on the upper part of the needle. The fuel of the volume NV1 follows the line NL2 towards the volume NV2, which corresponds to the existing volume between the needle and its seat. The line NL2 is defined with a section equivalent to the clearance between the needle wall and the nozzle wall, whereas the pressure force on the needle caused by the fuel present in volume NV2 is modelled with a new piston element (NP2). The volume NV2 feeds a valve with conical seat (OV3), which is associated with the restriction of the needle tip with its seat. The fuel that passes through that valve reaches the volume NV3, which finally feeds the six orifices of the nozzle. The parameters needed for characterizing each element of the nozzle model in AMESim (lines, volumes, pistons, etc.) have been obtained from silicon moulds [52] and the superposition of photos of the needle and this moulds. As an example of this procedure, Figure 4 shows three photos used to get the dimensional characteristics of the needle (left), the nozzle (center) and the volumes NV2 and NV3 (right). From this kind of pictures it is possible to know all the parameters required to define geometrically the 1D model of the nozzle (see Table 2).

Once each internal element of the injector is properly characterized in terms of its dimensions and hydraulic characteristics, the complete 1D model is capable to reproduce the main injector dynamics, including the instantaneous needle lift profile.

4.2 CFD validation in transient conditions in terms of mass flow rate.

Once the whole injector has been created in AMESim, the 1D model has been validated with experimental injection rates. Those injections rates were obtained using an Injection Rate Discharge Curve Indicator (RDCI) commercial system based on Bosch method [56]. Besides the injection rate, the AMESim model has provided the needle lift laws and the evolution of the injection pressure at the nozzle inlet. As Figure 5 shows, the injection pressure is not constant at all over the whole injection process. When the injection begins, the pressure falls suddenly around 15 MPa for the highest injection pressure (160 MPa) or 8 MPa for the case simulated at 80 MPa. That pressure drop remains with some oscillations until the moment the needle starts to move down. The pressure recovers as the needle moves down again to close the injector, due the fact that the mass flow entering the injector from the rail is higher than the one exiting through the nozzle. The sudden stop of the flow once the injector closes induces a pressure increase inside the injector, due to the conversion of kinetic energy into pressure. This phenomenon induces a pressure wave, which is still visible for some time after the needle closure, depending on the acoustic characteristics of the system.

The needle lift law obtained with AMESim for both injection pressures (160 and 80 MPa) and 3 MPa of backpressure can be seen in Figure 6. Although both laws could seem similar a priori, the scales of the horizontal axis are different. In any case, there is an initial stage where the needle moves up, a second stage where the needle keeps motionless and a last stage where the needle moves down again.

With the needle lift law obtained with AMESim, the complete injection process has been simulated for both pressure levels. Each simulation involves a considerable computational cost due to the length of the injection (≈1.5-2.5 ms) and the deformation of the cells during the motion of the needle, which slow down the calculation of every time step. As a reference, the case simulated at 160 MPa needed about 1370 CPU-hours in a cluster Xeon E5405@2GHz Quadcore 8 GB RAM. However, the real time was significantly reduced running the case in parallel.

The mass flow results for each pressure level have been plotted in Figure 7 together with the injection rate provided by AMESim and the one obtained experimentally. For both injection pressures, the AMESim injection rate (plotted in green line) fits considerably well the experimental injection rate (blue line) over the whole injection. CFD simulations with OpenFOAM overestimates a little the amount of fuel injected during the transient phases of opening and closing of the needle. That small deviation could be due to several reasons like the deformation of the needle at high injection pressure (not considered in this study) or the horizontal movement of the needle [31]. Nevertheless, attending to the central zone of the injection rate the differences among the experimental values and the CFD values coming from OpenFOAM is about 7-8 % for 160 MPa whereas it is almost negligible for the injection pressure of 80 MPa.

4.3 Analysis of transient cavitation structure.

As previously mentioned, one of the main advantages of using a moving mesh is the availability of results for any position of the needle between the maximum and minimum lift simulated. Thanks to that, it is possible to analyse with high accuracy the evolution of the cavitation appearance as the needle position changes. That transition is shown in Figure 8, where the vapour phase due to cavitation (in terms of the vapour fraction γ, previously defined) has been depicted for each needle position together with the evolution of mass flow at the nozzle outlet for an injection pressure of 160 MPa.

For the initial stages of the injection event (5 and 10 μm lift), most of the cavitation appearing in the nozzle is restricted to the needle seat area, while only a small portion of the orifice inlet presents cavitation. This is related to the low velocity existing inside the orifice at these conditions. As the needle moves up, the needle seat cavitation reduces significantly, and the length of the cavitation cloud inside the orifice increases. Up to a needle lift of 40 μm, the vapour phase located in the orifice extends only along the lower wall. The cavitating region in the orifice inlet grows on the sides as the needle goes up further (50 μm) due to the big amount of fuel coming from different areas in the sac. If the needle keeps moving up, the vapour is generated around all

the perimeter of the inlet section (60 μm) and spreads along the upper and lower part of the orifice simultaneously (65 μm). Afterwards, as the fuel comes into the orifice through the upper curvature radius, the vapour bubbles of the lower part disappear.

During the opening process of the injector, the direction of the fuel when it reaches the orifice changes, as shown in Figure 9. That figure represents the velocity field in the symmetry plane of the nozzle for five different needle lifts between 60 and 75 μm and shows the different paths follow by the fuel according to the needle position. As the needle moves up, the path of the flow before reaching the orifice gets away from the sac and from the lower curvature radius and gets closer to the nozzle wall and upper radius. That phenomenon can be easily seen comparing the lowest and the highest needle lifts shown in this figure (60 and 75 μm) where the near wall velocity of the fuel that has not reached the orifice changes from negligible values (60 μm) up to values close to 250 m/s (75 μm) . For low needle lifts, the strong area reduction in the needle seat accelerates the flow and generates enough kinetic energy to reach the sac. For high needle lifts, in contrast, the fuel does not accelerate in such a way as the area reduction in the needle seat is not so significant. Thus, the fuel does not have enough kinetic energy to penetrate up to the sac and goes into the orifice mainly from its upper part.

Obviously, the acceleration of the fuel at the needle seat comes together with its corresponding pressure drop, responsible for the phase change from liquid to vapour. As can be seen in Figure 10, the smaller the needle lift, the bigger the acceleration of the fuel and the pressure drop. This figure highlights the huge influence and the sensitivity of the needle position on the pressure field near the needle seat. When the needle is at 60 mm (left picture), the strong area reduction at the needle seat accelerates the flow as seen in Figure 9 and the pressure falls abruptly, generating vapour bubbles. However for a needle lift of 75 mm (right picture), as the area reduction at the needle seat is not so important, the pressure does not fall below the saturation pressure and all the fuel remains in liquid phase until reaching the orifice.

For a lower injection pressure (80 MPa), the transition of the cavitation zone from the lower to the upper section of the orifice could be considered as similar to the one previously analysed. These results are seen in Figure 11. Indeed, it can be seen how these results are very similar to those previously analysed for the 160 MPa case (Figure 8), with the only difference that the velocities in the 80 MPa conditions are lower, producing lower cavitation intensity and, as a consequence, limiting the extension of the cavitation area compared to the previous simulation.

Regarding the behaviour of the mass flow, it can be observed how some fluctuations appears precisely between 60 and 70 μm lift, when the transition of the cavitation area formation was observed. This is related to the fact that, during this transition, the cavitation area passes continuously from reaching the orifice outlet to not doing it, inducing an instantaneous distortion in the mass flow. This was not visible in the 160 MPa simulation since the intensity of the cavitation formation was higher and the cavitation area was reaching the orifice outlet during the complete simulation.

5. COMPARATIVE ANALYSIS OF THE INTERNAL FLOW WITH FIXED NEEDLE LIFT AND DYNAMIC MESH.

This section compares the differences in the study of the internal flow development with fixed needle lifts (stationary simulations at 10, 20, 30, 40, 50, 75 and 100 μm) and mesh motion (transient simulations). This comparison has been performed at two different levels of injection pressure (160 and 80 MPa) and keeping always a backpressure of 3 MPa.

5.1 Comparison in terms of the characteristics of the flow at the nozzle outlet.

Figures 12, 13 and 14 show the mass flow, momentum flux and effective velocity values obtained computationally with fixed needle lifts and moving mesh. For both pressure conditions, the differences found among the mass flow values provided by the code in its different versions are almost insignificant. Indeed, the averaged deviation between the results at fixed needle positions

and the transient simulation is 1.71% for the highest injection pressure (160 MPa) and 3.07% for the lowest injection pressure (80 MPa).

That conclusion can be extended for the momentum flux results, since for all the cases that can be directly compared (10, 20, 30, 40, 50, 75 and 100 μm) the differences are practically negligible. The maximum deviation between both kinds of simulations corresponds with a needle lift of 50 μm for an injection pressure of 160 MPa, where the difference is only 0.09 N.

As the effective velocity is calculated dividing the mass flow values by the momentum flux values [8], [57], no important differences can be expected among the values obtained with the code at fixed needle lifts and those obtained simulating the real movement of the needle. Thus, the effective velocity results represented in Figure 14 show that the averaged deviations are around 4.65% and 3.83% for the injection pressures 160 MPa and 80 MPa respectively.

Leaving aside the comparison between the values obtained with both approaches, the use of a moving mesh allows as well the estimation with more confidence of the needle position from where the needle stops having influence on the fuel characteristics at the nozzle outlet. Looking only at the steady values, it can be stated that this phenomenon is found for a needle lift between 50 and 75 μm. However, after simulating the opening process of the injector with the transient simulations of the code, it is possible to be more precise and accurate and define that phenomenon in a needle lift of 73-75 μm for both injection pressures.

5.2 Comparison in terms of cavitation development.

Once the good agreement between the values at the nozzle outlet predicted by the code considering the needle motion and those obtained at fixed lifts is checked, the differences in the cavitation development can be analysed. For that purpose, Figures 15 and 16 show the surface with vapour phase $\gamma > 0.1$ for both pressure levels (160 and 80 MPa).

Comparing the figures, both approaches show similar trends in general terms. For relatively high needle lifts (75 and 100 μm), the cavitation extends only to the upper part of the orifice, whereas

for needle lifts lower than 75 μm, cavitation is found in the needle seat and in the lower part of the orifice. However, looking in depth at the pictures corresponding to needle lifts smaller than 75 mm, it is possible to notice some differences with regard to the total volume of vapour generated in the needle seat. In particular, the simulations run with moving mesh show less fuel in vapour phase.

Those differences a priori could be considered as important for the development of the internal flow, but they do not seem to affect significantly the characteristics of the fuel at the nozzle exit, as seen in Figures 12-14. On the one hand, the mass flow remains constant as soon as cavitation starts regardless of the amount of vapour generated in the seat. On the other hand, despite of there is more volume of vapour, the reduction of friction with the walls due to its low viscosity only takes place near the needle seat. The rest of the vapour does not develop attached to the walls, so the friction losses keep constant and the momentum flux remains unaffected.

The influence of the needle motion on the internal flow and the cavitation development becomes more important for low needle lifts, where the needle speed stops being insignificant compared to the velocity of the fuel. In fact, the length of vapour phase obtained with moving mesh for 10 and 20 μm is significantly smaller as can be seen in Figure 15. Reducing the injection pressure up to 80 MPa (Figure 16), the velocity of the fluid reduces too and the influence of the needle speed increases even more. In this case, big differences in cavitation length can be noticed for 10, 20 and even 30 μm.

6. CONCLUSIONS

The current paper has focused on the analysis of the internal flow in a diesel injector nozzle comparing the characteristics of the flow at the nozzle outlet and the cavitation development with steady simulations at fixed needle positions against transient simulations with moving mesh. Those transient simulations have been possible thanks to the modification of the cavitation model implemented in OpenFOAM. The whole injection process (including the opening and closing

stages) has been simulated using the lift law and the injector pressure obtained from a model of the injector created in AMESim. From these studies, the following conclusions can be deduced:

- The differences in mass flow, momentum flux and effective velocity obtained with steady and transient simulations are below 7-8 % depending on the case. That means that, at least for the estimation of the characteristics of the flow at the nozzle exit, it would be enough to study the opening or closing process of the injector with steady simulations.
- Looking only at the results at fixed needle lifts (steady simulations) it is correct to state that the position of the needle from where the needle stops having influence on the characteristics of the fuel at the nozzle exit is between 50 and 75 μm. Nevertheless, after simulating with moving mesh the complete injector opening, the position can be determined with more accuracy, being between 73 and 75 μm.
- For needle lifts higher than 75 μm, the appearance of the cavitation with steady and transient simulations is similar. However, for needle lifts smaller than 75 μm, the length of the cavitation developed in the nozzle sac with moving mesh is slightly smaller. The influence of the needle motion increases for very small needle lifts (10 and 20 μm), where the speed of the needle cannot be considered as negligible compared to the velocity of the fuel.

7. REFERENCES

[1] A. Andriotis and M. Gavaises, "Influence of vortex flow and cavitation on near-nozzle diesel spray dispersion angle," *At. Sprays*, vol. 19, no. 3, pp. 247–261, 2009.

[2] R. Payri, F.J. Salvador, J. Gimeno, "Influence of injector technology on injection and combustion development-Part 2: Combustion analysis" *Applied Energy.*, vol. 88, no. 4 pp. 1130–1139, 2011.

[3] J,M. Luján, B. Tormos, F.J. Salvador, K. Galgar, "Comparative analysis of a DI diesel

fuelled with biodiesel blends during the European MVEG-A cycle: Preliminary Study (I)" *Biomass and Bioenergy*, vol. 33, no. 6-7, pp. 941–947, 2009.

[4] J. G. Hong, K. W. Ku, S. R. Kim, and C. W. Lee, "Effect of cavitation in circular nozzle and elliptical nozzles on the spray characteristic," *At. Sprays*, vol. 20, no. 10, pp. 877–886, 2010.

[5] R. Payri, F. J. Salvador, J. Gimeno, and O. Venegas, "Study of cavitation phenomenon using different fuels in a transparent nozzle by hydraulic characterization and visualization," *Exp. Therm. Fluid Sci.*, vol. 44, pp. 235–244, 2013.

[6] V. Bermúdez, R. Payri, F. J. Salvador, and A. H. Plazas, "Study of the influence of nozzle seat type on injection rate and spray behavior," *ImechE. J. Automob. Eng.*, vol. 219, no. 5, pp. 677–689, 2005.

[7] S. Molina, F. J. Salvador, M. Carreres, and D. Jaramillo, "A computational investigation on the influence of the use of elliptical orifices on the inner nozzle flow and cavitation development in diesel injector nozzles," *Energy Convers. Manag.*, vol. 79, pp. 114–127, 2014.

[8] R. Payri, J. M. Garcia-Oliver, F. J. Salvador, and J. Gimeno, "Using spray momentum flux measurements to understand the influence of diesel nozzle geometry on spray characteristics," *Fuel*, vol. 84, no. 5, pp. 551–561, 2005.

[9] J. J. Lopez, F. J. Salvador, O. A. De la Garza, and J. Arrègle, "A comprehensive study on the effect of cavitation on injection velocity in diesel nozzles," *Energy Convers. Manag.*, vol. 64, pp. 415–423, 2012.

[10] D. P. Schmidt and M. L. Corradini, "The internal flow of Diesel fuel injector nozzles: a review," *Int. J. Engine Res.*, vol. 2, no. 6, pp. 1–22, 2001.

[11] F. Payri, V. Bermúdez, R. Payri, and F. J. Salvador, "The influence of cavitation on the internal flow and the spray characteristics in diesel injection nozzles," *Fuel*, vol. 83, no.

4–5, pp. 419–431, 2004.

[12] V. Macian, R. Payri, X. Margot, and F. J. Salvador, "A CFD analysis of the influence of diesel nozzle geometry on the inception of cavitation," *At. Sprays*, vol. 13, pp. 579–604, 2003.

[13] J. Zhang, Q. Du, and Y. Yang, "Influence of Diesel Nozzle Geometry on Cavitation Using Eulerian Multi-Fluid Method," *Trasactions Tiajin Univ.*, vol. 16, no. 1, pp. 33–39, 2010.

[14] X. Zhang, J. Liu, and J. Wang, "Effect of fuel and nozzle geometry on the off-axis oscillation of needle in diesel injectors using high-speed X-ray phase contrast imaging," *J. Instrum.*, vol. 11, no. 5, pp. C05015–C05015, 2016.

[15] S. Som, A. I. Ramírez, D. E. Longman, and S. K. Aggarwal, "Effect of nozzle orifice geometry on spray, combustion, and emission characteristics under diesel engine conditions," *Fuel*, vol. 90, no. 3, pp. 1267–1276, 2011.

[16] F. J. Salvador, M. Carreres, D. Jaramillo, and J. Martínez-López, "Comparison of microsac and VCO diesel injector nozzles in terms of internal nozzle flow characteristics," *Energy Convers. Manag.*, vol. 103, pp. 284–299, 2015.

[17] F. J. Salvador, M. Carreres, D. Jaramillo, and J. Martínez-López, "Analysis of the combined effect of hydrogrinding process and inclination angle on hydraulic performance of diesel injection nozzles," *Energy Convers. Manag.*, vol. 105, pp. 1352–1365, 2015.

[18] G. Stumpp and M. Ricco, "Common Rail - An attractive fuel injection system for passenger car DI Diesel engines," *SAE Tech. Pap. 960870*, 1996.

[19] S. Mendez and B. Thirouard, "Using Multiple Injection Strategies in Diesel Combustion: Potential to Improve Emissions, Noise and Fuel Economy Trade-Off in Low CR Engines," *SAE Tech. Pap. 2008-01-1329*, vol. 1, no. 1, pp. 662–674, 2008.

[20] Y. Mingfa and W. Hu, “Experimental Study of Multiple Injections and Coupling Effects of Multi-Injection and EGR in a HD Diesel Engine,” *SAE Tech. Pap. 2009-01-2807*, 2009.

[21] M. Blessing, G. König, C. Krüger, U. Michels, and V. Schwarz, “Analysis of flow and cavitation phenomena in diesel injection nozzles and its effects on spray and mixture formation,” *SAE Tech. Pap. 2003-01-1358*, 2003.

[22] R. Masuda, T. Fuyuto, M. Nagaoka, E. Von Berg, and R. Tatschl, “Validation of Diesel Fuel Spray and Mixture Formation from Nozzle Internal Flow Calculation,” *SAE Tech. Pap. 2005-01-2098*, 2005.

[23] O. Soriano, M. Sommerfeld, and A. Burkhardt, “Validation of a cavitation and turbulence induced model for the primary breakup of diesel jets,” in *ILASS - Europe 2008, 21 Annual Conference on Liquid Atomization and Spray Systems*, 2008.

[24] S. Som, S. K. Aggarwal, E. M. El-Hannouny, and D. E. Longman, “Investigation of nozzle flow and cavitation characteristics in a diesel injector,” *J. Eng. Gas Turbines Power*, vol. 132, no. 4, p. 42802, 2010.

[25] F. Incorporated, “Fluent v. 5.0 user’s guide, vol. 2,” 1998.

[26] F. J. Salvador, J. Martínez-López, M. Caballer, and C. De Alfonso, “Study of the influence of the needle lift on the internal flow and cavitation phenomenon in diesel injector nozzles by CFD using RANS methods,” *Energy Convers. Manag.*, vol. 66, pp. 246–256, 2013.

[27] J. M. Desantes, F. J. Salvador, M. Carreres, and J. Martínez-López, “Large-eddy simulation analysis of the influence of the needle lift on the cavitation in diesel injector nozzles,” *Proc. Inst. Mech. Eng. Part D J. Automob. Eng.*, vol. 229, no. 4, pp. 407–423, 2014.

[28] T. Oda, Y. Goda, S. Kanaike, K. Aoki, and K. Ohsawa, “Experimental Study about

internal Cavitating Flow and Primary Atomization of a Large-Scaled VCO Diesel Injector with Eccentric Needle," *11th Trienn. Int. Annu. Conf. Liq. At. Spray Syst.*, vol. 132, 2009.

[29] F. J. Salvador, J. Martínez-López, J. V. Romero, and M. D. Roselló, "Study of the influence of the needle eccentricity on the internal flow in diesel injector nozzles by computational fluid dynamics calculations," *Int. J. Comput. Math.*, vol. 91, no. June, pp. 24–31, 2013.

[30] M. Battistoni, Q. Xue, S. Som, and E. Pomraning, "Effect of Off-Axis Needle Motion on Internal Nozzle and Near Exit Flow in a Multi-Hole Diesel Injector," *SAE Int. J. Fuels Lubr.*, vol. 7, no. 1, pp. 2014-01–1426, Apr. 2014.

[31] O. Chiavola and F. Palmieri, "Modeling Needle Motion Influence on Nozzle Flow in High Pressure Injection System," *SAE Tech. Pap.*, 2007.

[32] LMS, "Imagine.Lab AMESim v.10. User's manual." 2010.

[33] J. W. Lee, K. D. Min, K. Y. Kang, C. Bae, E. Giannadakis, M. Gavaises, and C. Arcoumanis, "Effect of piezo-driven and solenoid-driven needle opening of common-rail diesel injectors on internal nozzle flow and spray development," *Int. J. Engine Res.*, vol. 7 (6), pp. 489–502, 2006.

[34] R. Marcer, C. Audiffren, A. Viel, B. Bouvier, A. Walbott, and B. Argueyrolles, "Coupling 1D System AMESim and 3D CFD EOLE models for Diesel Injection Simulation Renault," in *ILASS - Europe 2010, 23rd Annual Conference on Liquid Atomization and Spray Systems*, 2010, no. September, pp. 1–10.

[35] F. J. Salvador, S. Hoyas, R. Novella, and J. Martínez-López, "Numerical simulation and extended validation of two-phase compressible flow in diesel injector nozzles," *Proc. Inst. Mech. Eng. Part D J. Automob. Eng.*, vol. 225, no. 4, pp. 545–563, 2011.

[36] D. P. Schmidt, C. J. Rutland, and M. L. Corradini, "A fully compressible two-

dimensional model of high speed cavitating nozzles," *At. Sprays*, vol. 9, pp. 255–276, 1999.

[37] F. J. Salvador, J. V. Romero, M. D. Roselló, and J. Martínez-López, "Validation of a code for modeling cavitation phenomena in Diesel injector nozzles.," *Math. Comput. Model.*, vol. 52, no. 7–8, pp. 1123–1132, 2010.

[38] F. J. Salvador, J. Martínez-López, J. V. Romero, and M. D. Roselló, "Computational study of the cavitation phenomenon and its interaction with the turbulence developed in diesel injector nozzles by Large Eddy Simulation (LES)," *Math. Comput. Model.*, vol. 57, no. 7–8, pp. 1656–1662, 2013.

[39] F. J. Salvador, D. Jaramillo, J. V. Romero, and M. D. Roselló, "Using a homogeneous equilibrium model for the study of the inner nozzle flow and cavitation pattern in convergent-divergent nozzles of diesel injectors," *J. Comput. Appl. Math.*, vol. 309, pp. 630–641, 2015.

[40] F. J. Salvador, J. Martínez-López, J. V. Romero, and M. D. Roselló, "Influence of biofuels on the internal flow in diesel injector nozzles," *Math. Comput. Model.*, vol. 54, no. 7–8, pp. 1699–1705, 2011.

[41] G. B. Wallis, "One-dimensional two-phase flow," *McGraw-Hill*, 1969.

[42] M. Chung, S. Park, and H. Lee, "Sound speed criterion for two-phase critical flow," *J. Sound Vib.*, pp. 13–26, 2004.

[43] A. Sou, S. Hosokawa, A. Tomiyama, and T. Akio, "Effects of cavitation in a nozzle on liquid jet atomization," *Int. J. Heat Mass Transf.*, vol. 50, no. 17–18, pp. 3575–3582, 2007.

[44] Z. He, W. Zhong, Q. Wang, Z. Jiang, and Z. Shao, "Effect of nozzle geometrical and dynamic factors on cavitating and turbulent flow in a diesel multi-hole injector nozzle," *Int. J. Therm. Sci.*, vol. 70, pp. 132–143, 2013.

[45] H. Taghavifar, S. Khalilarya, S. Jafarmadar, and H. Taghavifar, “A RANS simulation toward the effect of turbulence and cavitation on spray propagation and combustion characteristics,” *Theor. Comput. Fluid Dyn.*, vol. 30, no. 4, pp. 349–362, 2016.

[46] Q. Xue, S. Som, M. Battistoni, S. Quan, P. K. Senecal, E. Pomraning, and D. P. Schmidt, “Eulerian CFD Modeling of Coupled Nozzle Flow and Spray with Validation Against X-Ray Radiography Data,” *SAE Int. J. Engines*, vol. 7, no. 2, pp. 1061–1072, 2014.

[47] J. Reveillon, C. Péra, and Z. Bouali, “Examples of the potential of DNS for the understanding of reactive multiphase flows,” *Int. J. Spray …*, pp. 1–30, 2011.

[48] U. Piomelli, “Large-eddy simulation: achievements and challenges,” *Prog. Aerosp. Sci.*, pp. 335–362, 1999.

[49] E. de Villiers, “The Potential of Large Eddy Simulation for the Modeling of Wall Bounded Flows,” Department of Mechanical Engineering. Imperial College of Science, Technology and Medicine, 2006.

[50] H. K. Versteeg and W. Malalasekera, “An introduction to computational fluid dynamics,” *Longman Sci. Tech.*, 1995.

[51] V. Yakhot and S. Orszag, “Renormalization group analysis of turbulence. basic theory,” *J. Sci. Comput.*, vol. 1, no. 1, pp. 3–51, 1986.

[52] V. Macian, V. Bermúdez, R. Payri, and J. Gimeno, “New technique for determination of internal geometry of a Diesel nozzle with the use of silicone methodology,” *Exp. Tech.*, vol. 27, no. April, pp. 39–43, 2003.

[53] M. Gavaises, A. Andriotis, D. Papoulias, N. Mitroglou, and A. Theodorakakos, “Characterization of string cavitation in large-scale Diesel nozzles with tapered holes,” *Phys. Fluids*, vol. 21, no. 5, p. 52107, 2009.

[54] Z. He, G. Guo, X. Tao, W. Zhong, X. Leng, and Q. Wang, “Study of the effect of nozzle

hole shape on internal flow and spray characteristics," *Int. Commun. Heat Mass Transf.*, vol. 71, pp. 1–8, 2016.

[55] F. J. Salvador, J. Gimeno, J. De la Morena, "Using one-dimensional modeling to analyze the influence of the use of biodiesels on the dynamic behavior of solenoid-operated injectors in common rail systems: Results of the simulations and discussion," *Energy Convers. Manag.*, vol. 54, no. 1, pp. 122–132, 2012.

[56] W. Bosch, "The Fuel Rate Indicator: a New Measuring Instrument for Display of the Characteristics of Individual Injection," *SAE Pap. 660749*, 1966.

[57] L. Postrioti, F. Mariani, and M. Battistoni, "Experimental and numerical momentum flux evaluation of high pressure Diesel spray," *Fuel*, vol. 98, pp. 149–163, 2012.

8. ACKNOWLEDGMENTS

This work was partly sponsored by "*Ministerio de Economa y Competitividad*", of the Spanish Government, in the frame of the Project "*Estudio de la interacción chorro-pared en condiciones realistas de motor*", Reference *TRA2015-67679-c2-1-R*. The authors would like also to thank the computer resources, technical expertise and assistance provided by Universidad de Valencia in the use of the supercomputer "*Tirant*".

LIST OF TABLE AND FIGURE CAPTIONS

Table 1: Fuel properties in liquid and vapour phase

Table 2: Dimensional values used in AMESim for the nozzle model.

Figure 1: Mesh of the simulated domain.

Figure 2: Deformation of the mesh for three different needle positions: high lift, intermediate lift and low needle lift.

Figure 3: Model of the nozzle implemented in AMESim.

Figure 4: Photo of the needle (left), photo of the silicone mould (center) and superposition of poth pictures for nozzle characterization (right).

Figure 5: Evolution of the injection pressure provided by AMESim. Energizing times of injector are 1ms and 2ms for 160 MPa and 80 MPa of injection pressure, respectively.

Figure 6: Needle lift law obtained with AMESim. Energizing times of injector are 1ms and 2ms for 160 MPa and 80 MPa of injection pressure, respectively.

Figure 7: Comparison of the injection rates obtained with OpenFOAM (red line), AMESim (green line) and experimentally (blue line). Energizing times of injector are 1ms and 2ms for 160 MPa and 80 MPa of injection pressure, respectively.

Figure 8: Evolution of the mass flow and cavitation development with moving mesh for P_{inj} = 160 MPa and P_{back} = 3 MPa.

Figure 9: Velocity field in the middle plane of the nozzle for different needle lifts at P_{inj} = 160 MPa.

Figure 10: Pressure field at P_{inj} = 160 MPa and P_{back} = 3 MPa for two different needle lifts: 60 μm (left) and 75 μm (right).

Figure 11: Evolution of the mass flow and cavitation development with moving mesh for P_{inj} = 80 MPa and P_{back} = 3 MPa.

Figure 12: Mass flow comparison with fixed needle lifts and moving mesh.

Figure 13: Momentum flux comparison with fixed needle lifts and moving mesh.

Figure 14: Effective velocity comparison with fixed needle lifts and moving mesh.

Figure 15: Cavitation at fixed needle lifts and moving mesh for P_{inj} = 160 MPa and P_{back} = 3 MPa.

Figure 16: Cavitation at fixed needle lifts and moving mesh for P_{inj} = 80 MPa and P_{back} = 3 MPa.

	Liquid phase	Vapour phase
Density [kg/m^3]	830	0.1361
Viscosity [kg/ms]	$3.67 \cdot 10^{-3}$	$5.95 \cdot 10^{-6}$
Compressibility [s/m^2]	$5 \cdot 10^{-7}$	$2.5 \cdot 10^{-6}$

Table 1: Fuel properties in liquid and vapour phase

Element	Length (mm)	Diameter (mm)	Volume (cm^3)	Mass (g)
NL1	15	2.16	-	-
FF12	12.6	4	-	-
NV1	-	-	0.032	
NM	-	-	-	3.1
NP1	-	4	-	-
NL2	27	2.4	-	-
NV2	-	-	0.005	-
NP2	-	3.04	-	-
OV3	-	0.57	-	-
NV3	-	-	5.84e-5	-
Orifices	-	0.17	-	-

Table 2: Dimensional values used in AMESim for the nozzle model.

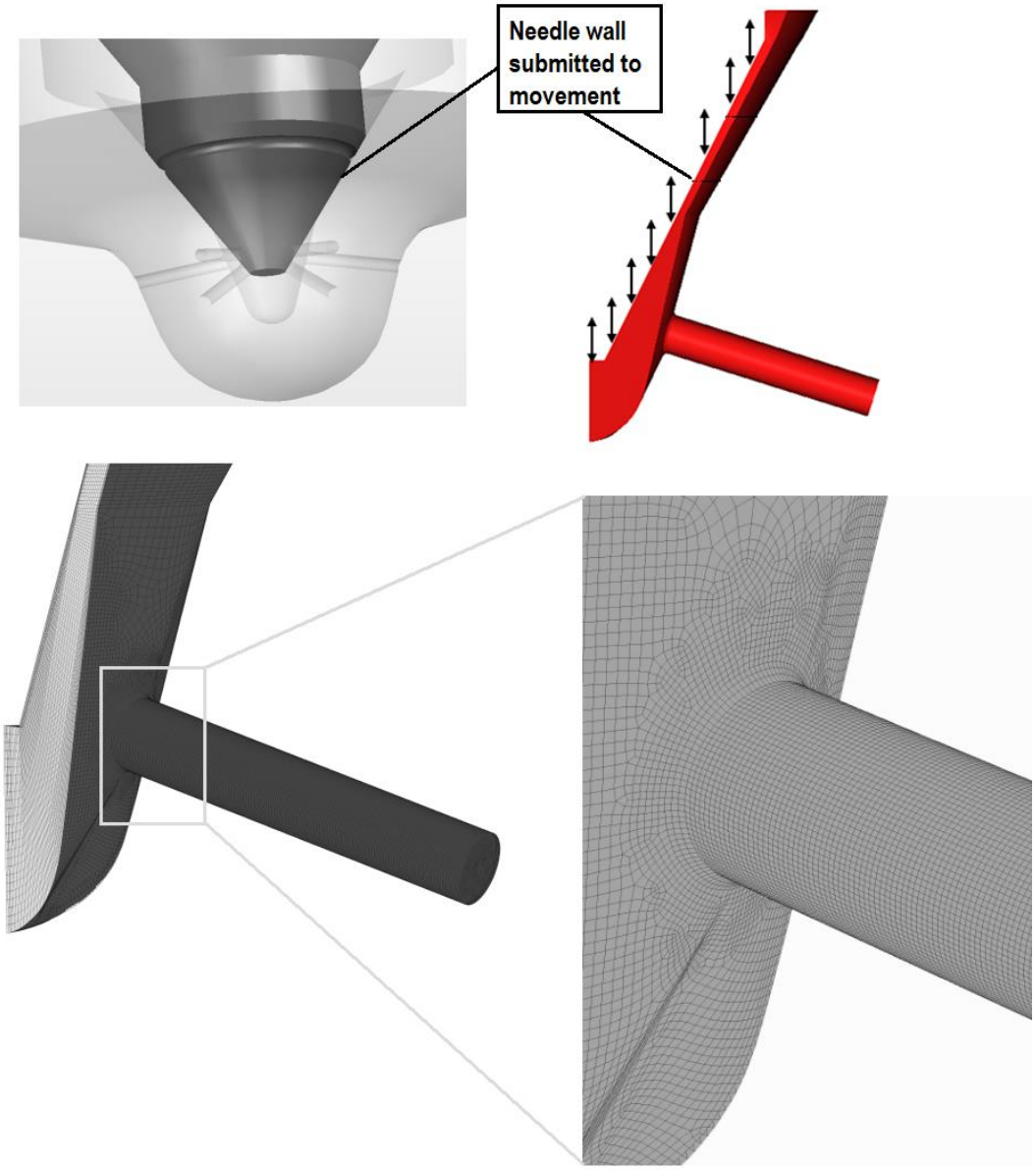

Figure 1: Mesh of the simulated domain.

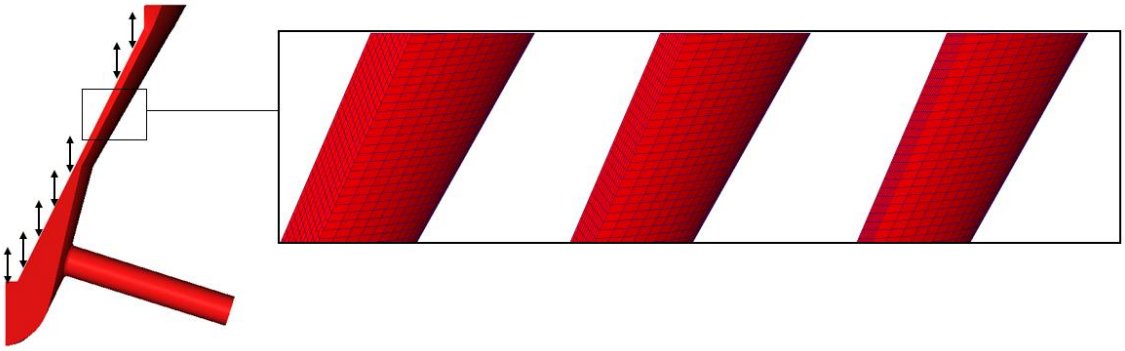

Figure 2: Deformation of the mesh for three different needle positions: high lift, intermediate lift and low needle lift.

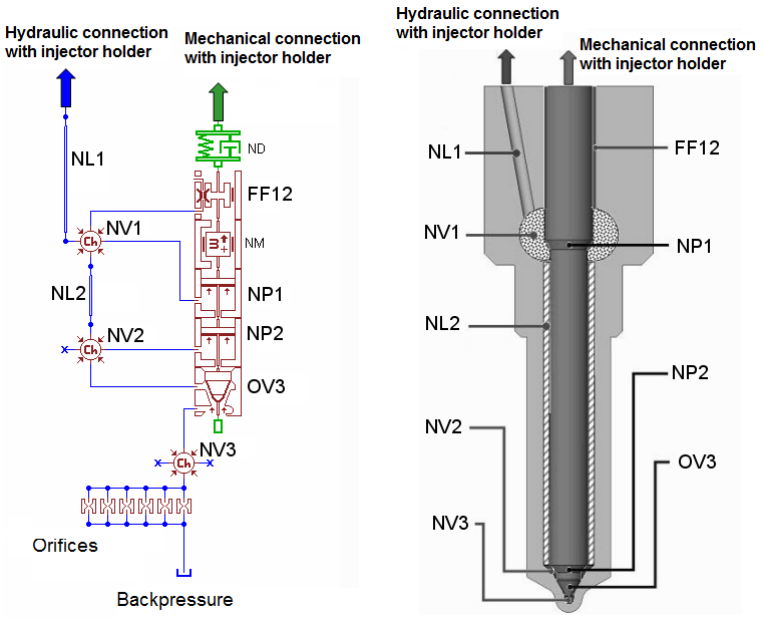

Figure 3: Model of the nozzle implemented in AMESim.

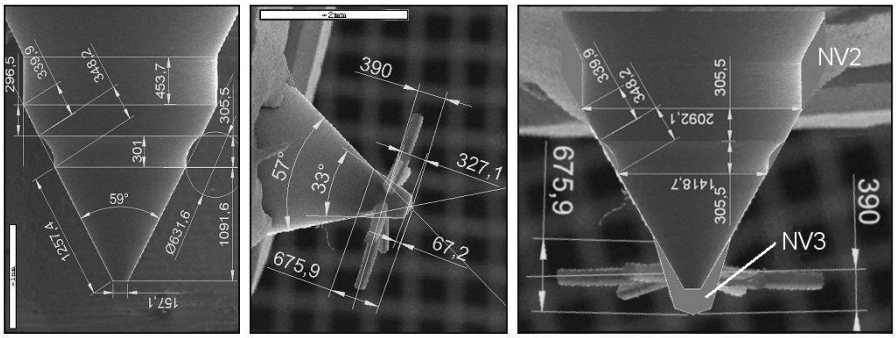

Figure 4: Photo of the needle (left), photo of the silicone mould (center) and superposition of poth pictures for nozzle characterization (right).

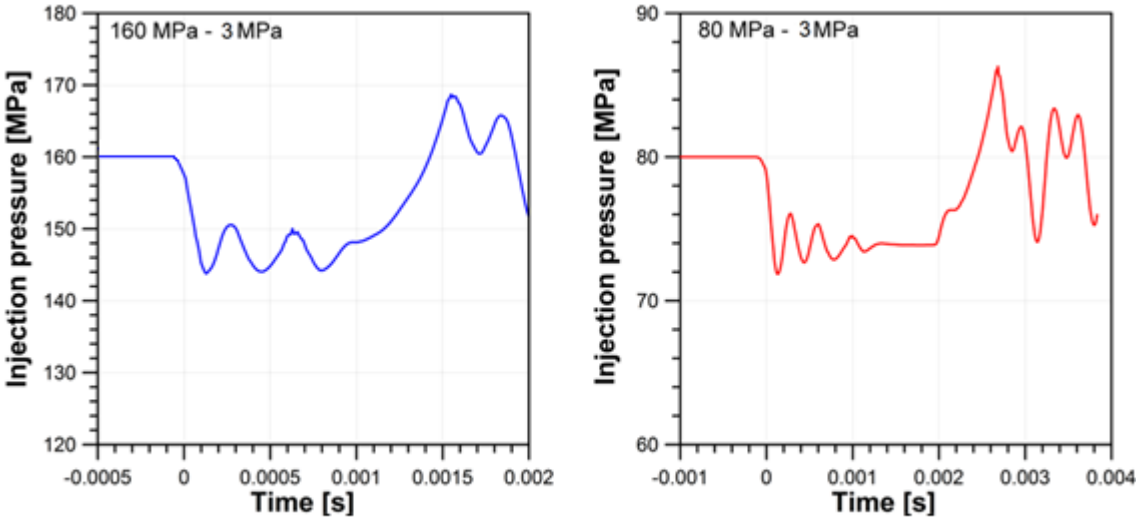

Figure 5: Evolution of the injection pressure provided by AMESim. Energizing times of the injector are 1 ms and 2 ms for 160 MPa (left) and 80 MPa (right) of injection pressure, respectively.

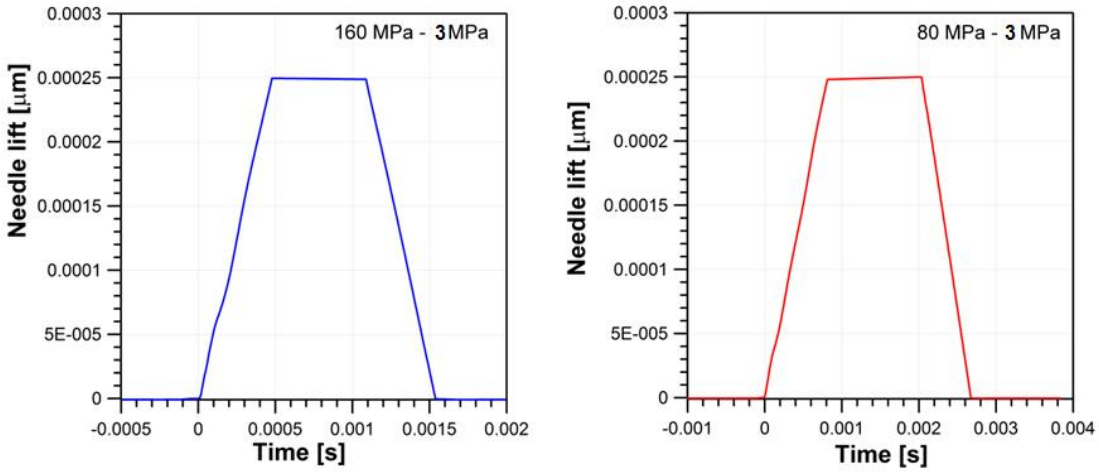

Figure 6: Needle lift law obtained with AMESim. Energizing times of the injector are 1 ms and 2 ms for 160 MPa (left) and 80 MPa (right) of injection pressure, respectively.

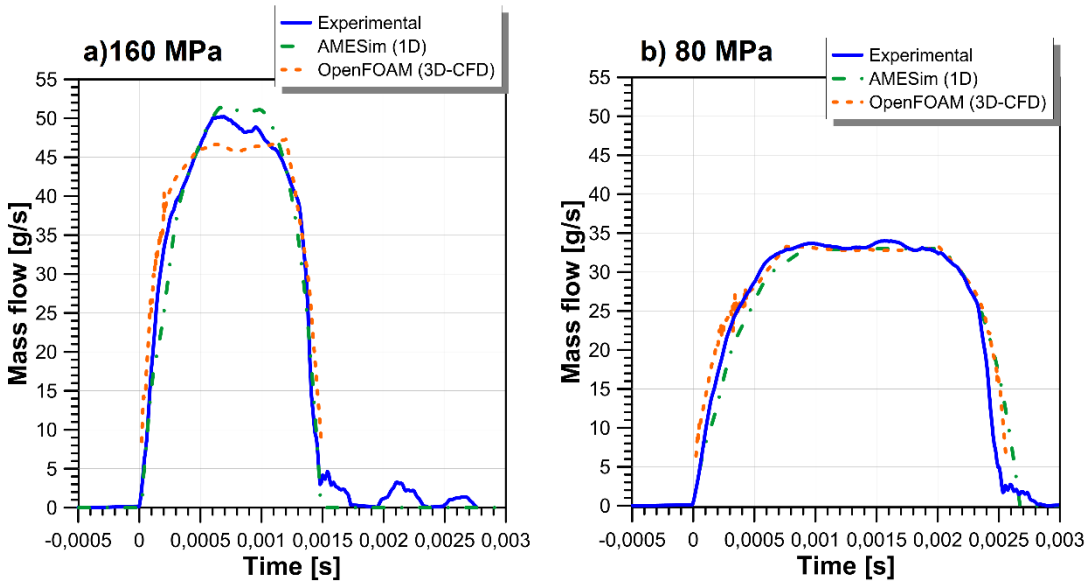

Figure 7: Comparison of the injection rates obtained with OpenFOAM (red line), AMESim (green line) and experimentally (blue line). Energizing times of the injector are 1 ms and 2 ms for 160 MPa (left) and 80 MPa (right) of injection pressure, respectively.

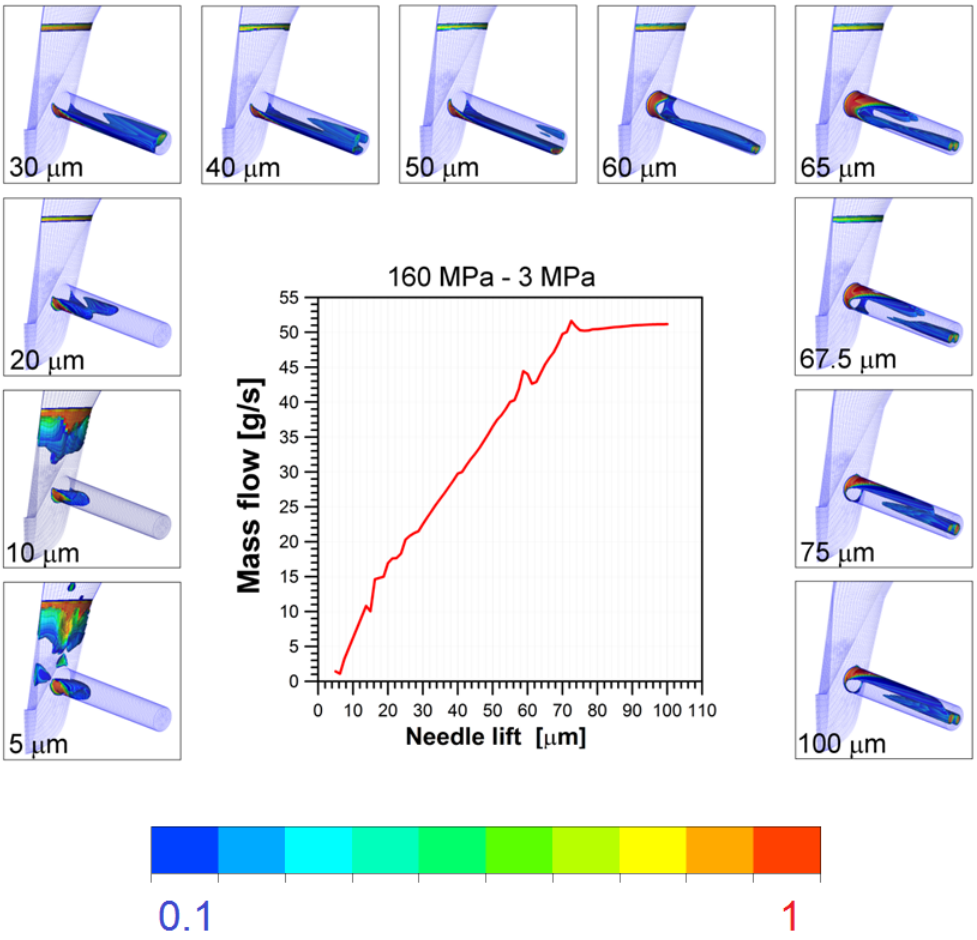

Figure 8: Evolution of the mass flow and cavitation development (contours of void fraction, γ) with moving mesh for P_{inj} = 160 MPa and P_{back} = 3 MPa.

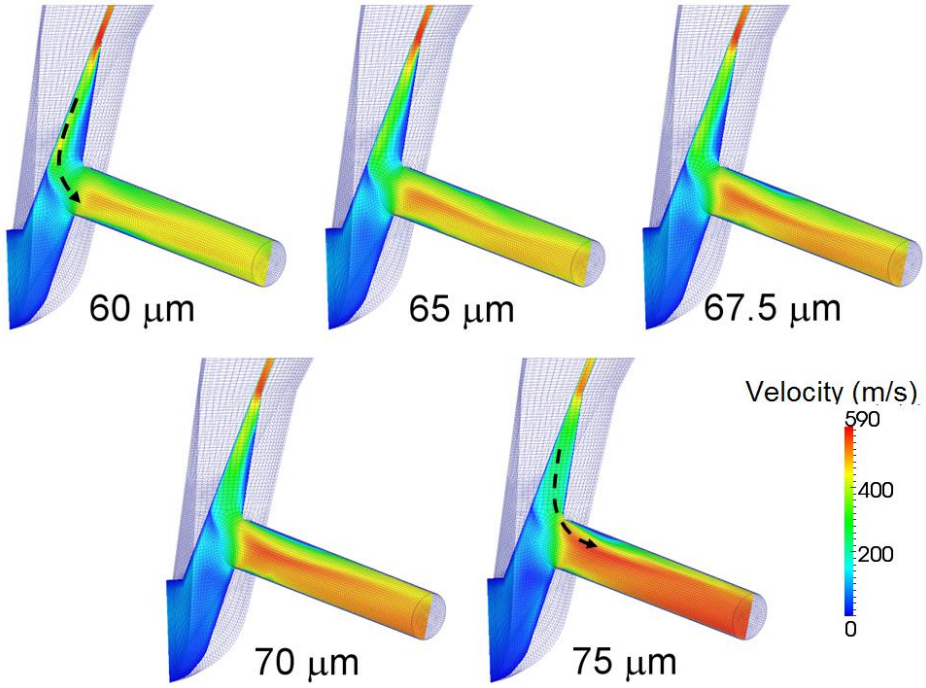

Figure 9: Velocity field in the middle plane of the nozzle for different needle lifts at P_{inj} = 160 MPa and P_{back} = 3 MPa.

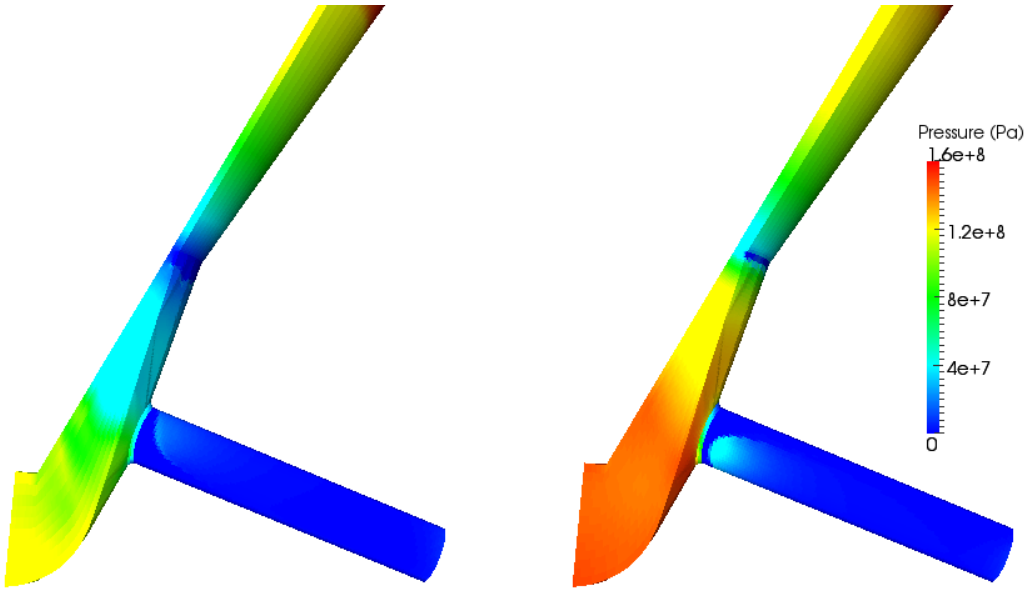

Figure 10: Pressure field at P_{inj} = 160 MPa and P_{back} = 3 MPa for two different needle lifts: 60 μm (left) and 75 μm (right).

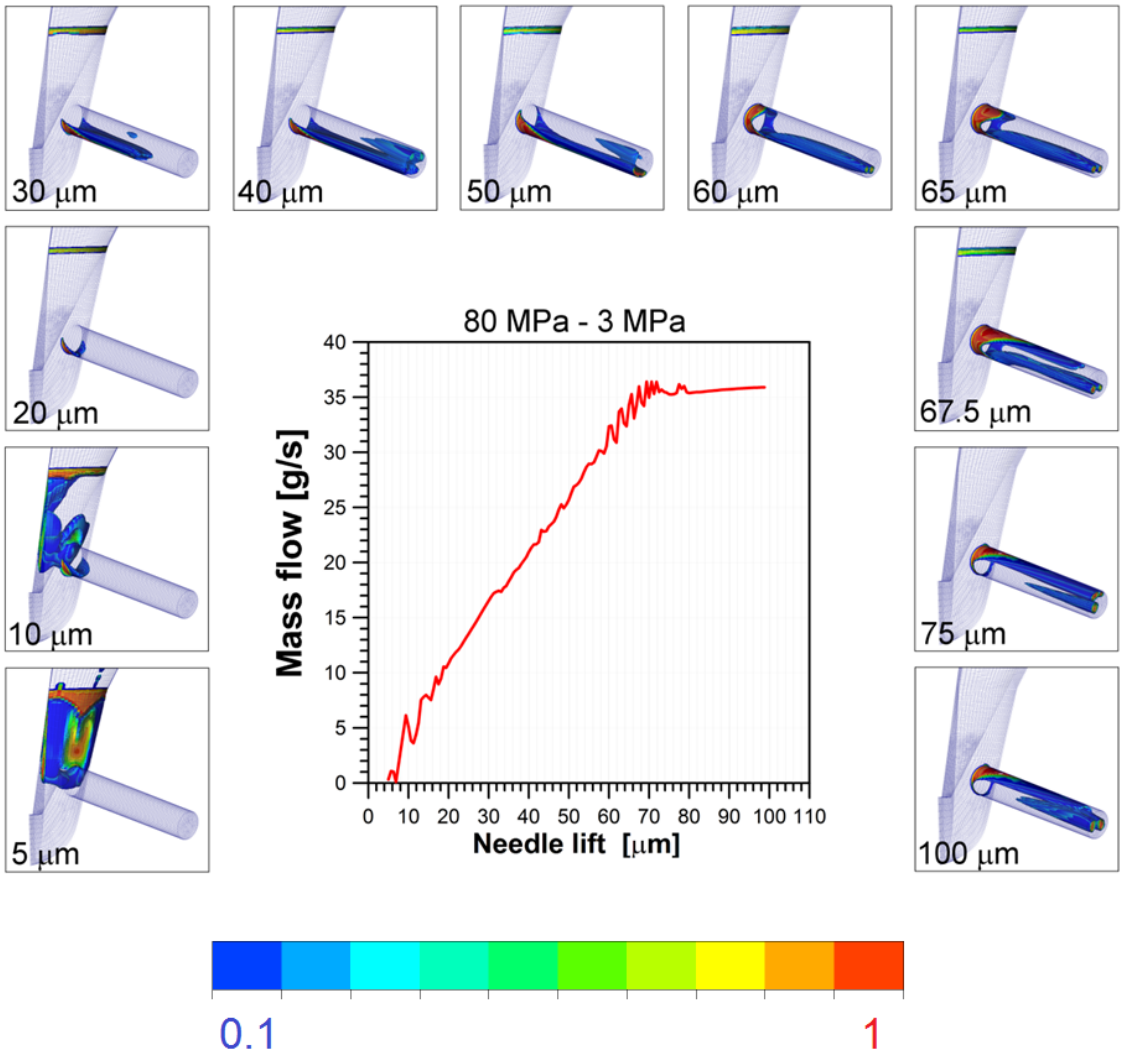

Figure 11: Evolution of the mass flow and cavitation development (contours of void fraction, γ) with moving mesh for P_{inj} = 80 MPa and P_{back} = 3 MPa.

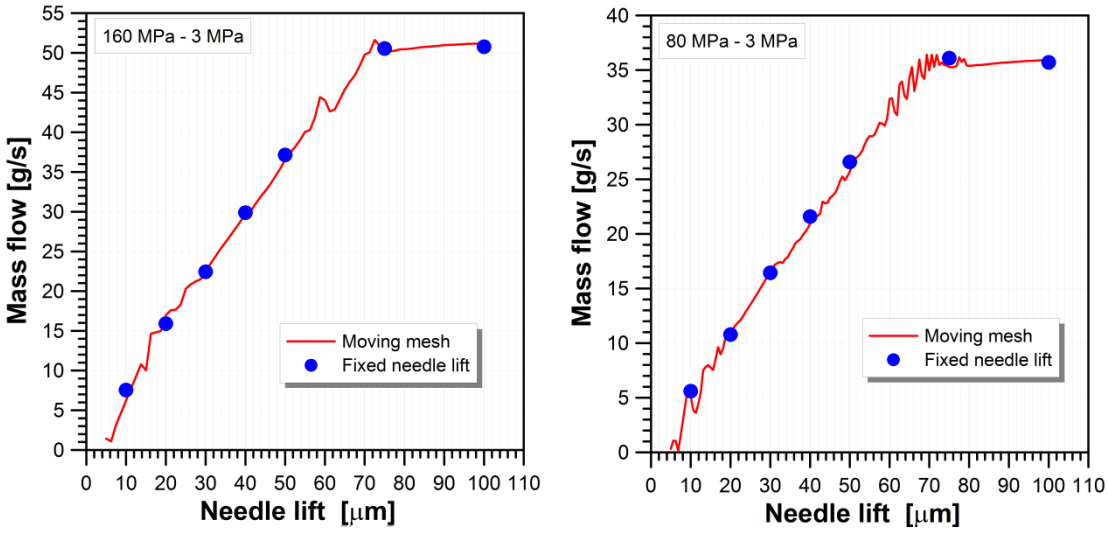

Figure 12: Mass flow comparison with fixed needle lifts and moving mesh.

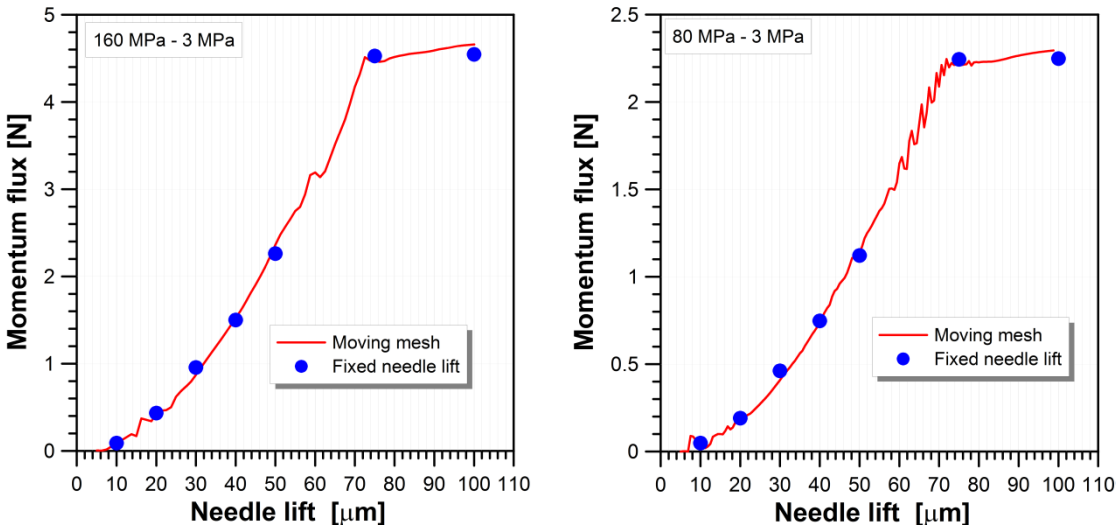

Figure 13: Momentum flux comparison with fixed needle lifts and moving mesh.

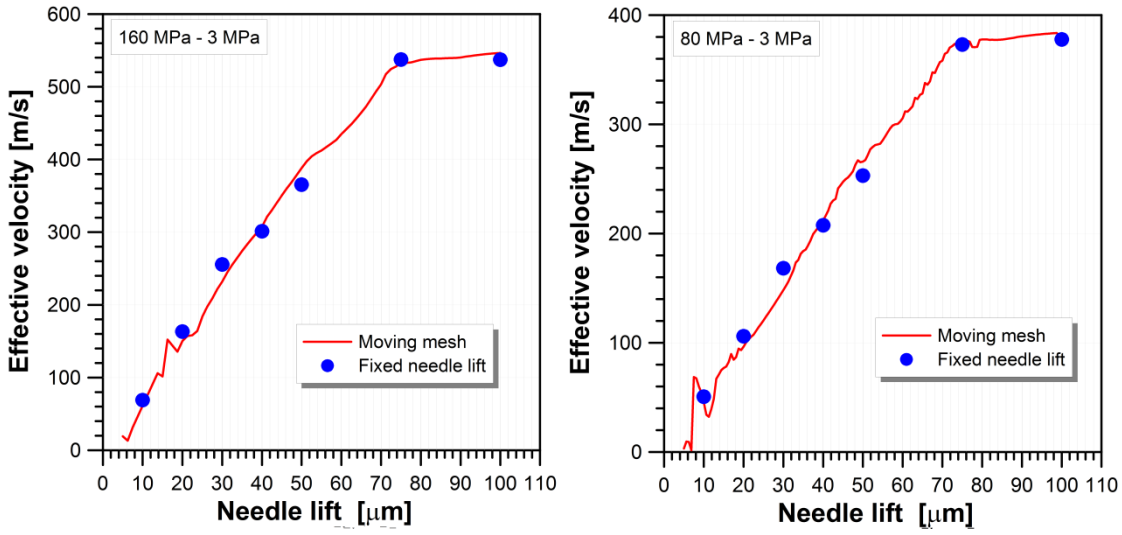

Figure 14: Effective velocity comparison with fixed needle lifts and moving mesh.

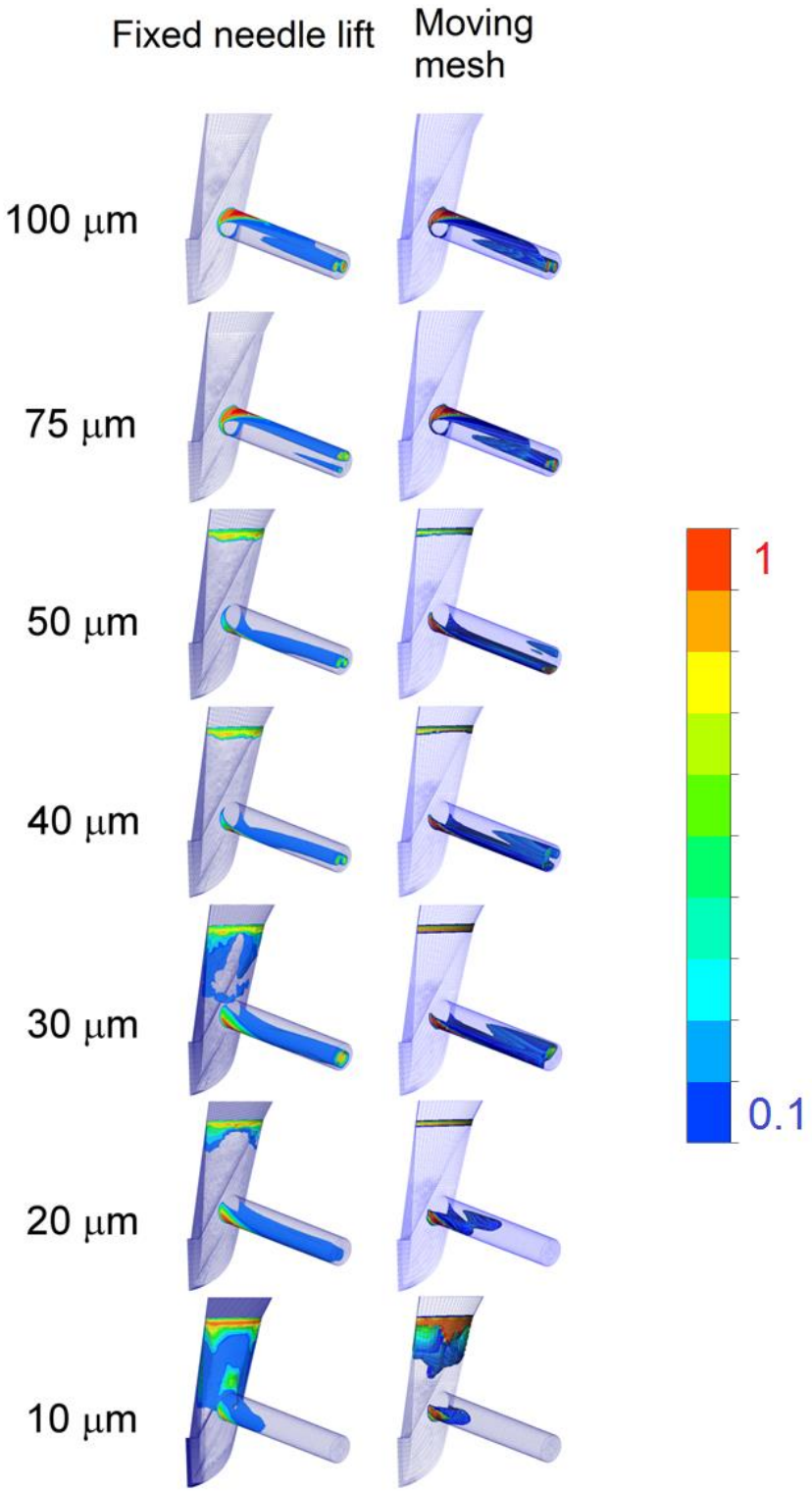

Figure 15: Cavitation at fixed needle lifts and moving mesh for P_{inj} = 160 MPa and P_{back} = 3 MPa. Contours of void fraction, γ

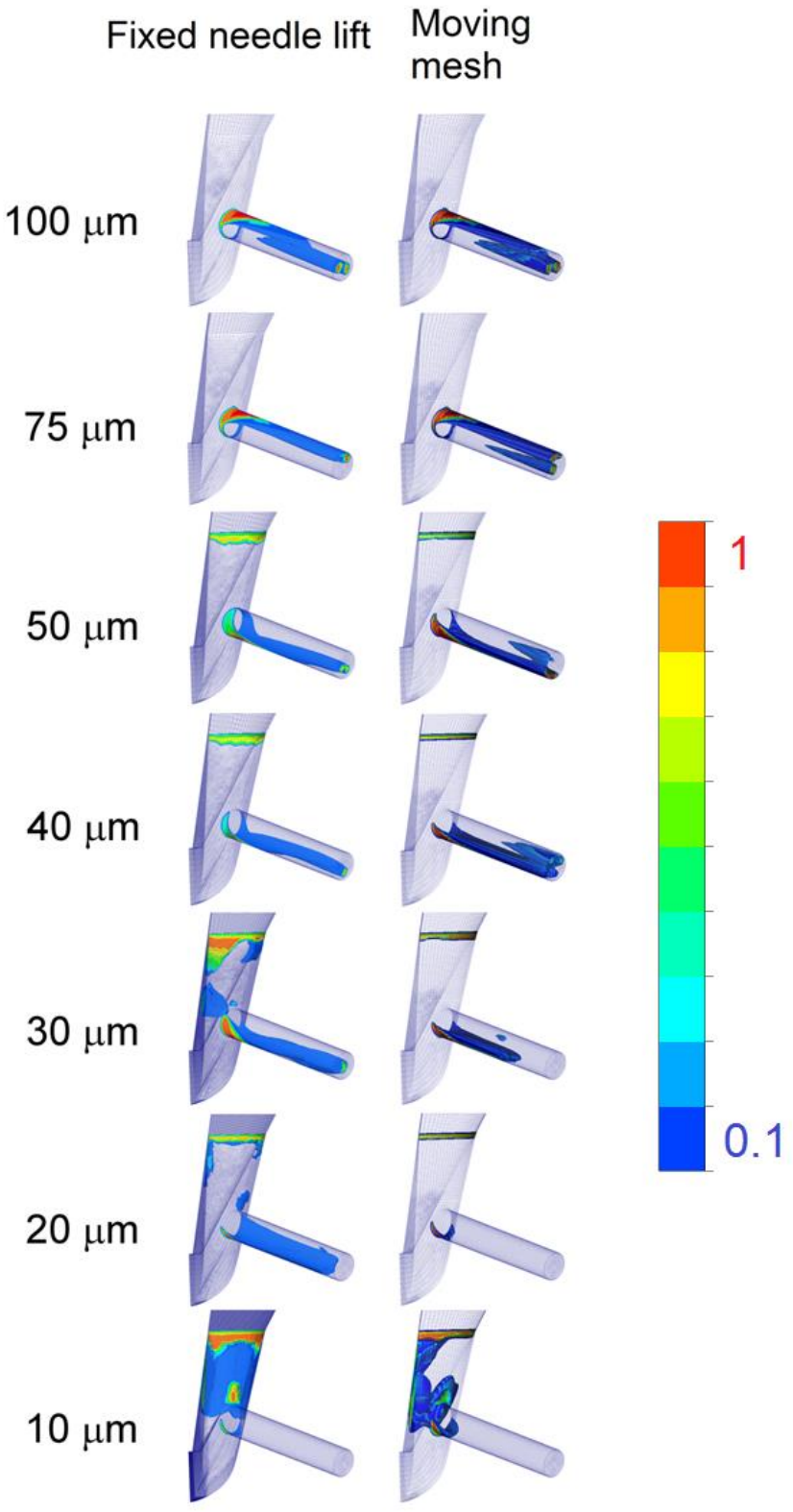

Figure 16: Cavitation at fixed needle lifts and moving mesh for P_{inj} = 80 MPa and P_{back} = 3 MPa. Contours of void fraction, γ.